

Tip/Tilt Optimizations for Polynomial Apodized Vortex Coronagraphs on Obscured Telescope Pupils

Kevin Fogarty^{a,b}, Laurent Pueyo^b, Johan Mazoyer^{a,b}, Mamadou N'Diaye^{c,b}

^aJohns Hopkins University Department of Physics and Astronomy, 3400 N. Charles St, Baltimore, USA;

^bSpace Telescope Science Institute, 3700 San Martin Dr, Baltimore, USA;

^cUniversité Côte d'Azur, Observatoire de la Côte d'Azur, CNRS, Laboratoire Lagrange, Bd de l'Observatoire, CS 34229, 06304 Nice cedex 4, France

ABSTRACT

Obstructions due to large secondary mirrors, primary mirror segmentation, and secondary mirror support struts all introduce diffraction artifacts that limit the performance offered by coronagraphs. However, just as vortex coronagraphs provides theoretically ideal cancellation of on-axis starlight for clear apertures, the Polynomial Apodized Vortex Coronagraph (PAVC) completely blocks on-axis light for apertures with central obscurations, and delivers off-axis throughput that improves as the topological charge of the vortex increases. We examine the sensitivity of PAVC designs to tip/tilt aberrations and stellar angular size, and discuss methods for mitigating these effects. By imposing additional constraints on the pupil plane apodization, we decrease the sensitivity of the PAVC to the small positional shifts of the on-axis source induced by either tip/tilt or stellar angular size; providing a route to overcoming an important hurdle facing the performance of vortex coronagraphs on telescopes with complicated pupils.

Keywords: Vector Vortex Coronagraph, On-Axis Telescopes, PIAA, Earthlike Exoplanet Imaging

1. INTRODUCTION

In order to take full advantage of planned and proposed large space observatories for high contrast imaging, it will be necessary to design coronagraphs suited to telescopes with obstructed apertures. Observatories such as WFIRST provide the sensitivity and resolution necessary to directly image sub-Jovian exoplanets, while proposals such as LUVOIR will allow for direct observations of terrestrial exoplanets.^{1–3} However, these telescopes, as well as large-aperture ground based telescopes, feature pupils with central obstructions due to secondary mirrors as well as features such as segment gaps and obstructions due to support struts which are collectively known as ‘spiders’.^{4–6} Central obstructions and spiders severely limit the ability of coronagraphs designed for un-obscured pupils to suppress starlight; therefore, exploiting the potential ability of future observatories to directly image exoplanets will require coronagraphs specifically designed for complicated pupil geometries.^{7–17}

In Fogarty et al. 2017¹⁸ (hereafter Paper I), we introduced the Polynomial Apodized Vortex Coronagraph (PAVC), which addresses the challenge posed by large central obstructions. The PAVC uses a pupil plane apodization to enable the vortex coronagraph to retain theoretically ideal starlight suppression¹⁹ in the presence of central obstructions while maintaining high off-axis source throughput. PAVC designs are available for all vortex topological charges (see Section 2.1 for a discussion of topological charge). In particular, the PAVC6 (PAVC with vortex topological charge 6), was shown to be robust to the central obstructions imposed by large secondary mirrors— the PAVC6 delivers ~ 50% encircled energy (E.E.) throughput and ~ 65% total energy (T.E.) throughput (T.E. throughput is the total flux in the image plane from an off-axis source, E.E. throughput is the flux measured in an aperture of radius $0.7 \lambda/D$; both definitions of throughput refer to flux measured relative to what would be observed by the same telescope with no coronagraph) for a telescope with a secondary mirror radius, R_S , that is 30% of the primary mirror radius, R_P .

Further author information: (Send correspondence to K. Fogarty)

K. Fogarty: E-mail: kfogarty@stsci.edu

In addition to ideal starlight suppression, vortex coronagraphs provide small inner working angles (IWAs) and can be manufactured to be achromatic.^{20–23} The PAVC allows coronagraph designs to take advantage of these properties with centrally obstructed pupils, and can be combined with techniques that correct for spiders. For example, combining the PAVC6 with the ACAD-OSM (Active Correction of Aperture Discontinuities- Optimized Stroke Minimization) technique discussed in Mazoyer et al. 2016,²⁴ allows one to correct for both a central obscuration and spiders by combining the PAVC with deformable mirror (DM) beam-shaping that mitigates the impact of spiders on starlight suppression. Likewise, Ruane et al. 2016²⁵ finds pupil apodizations for complicated apertures that converge on PAVC apodization functions when the aperture is obstructed by a secondary mirror.

While promising, vortex coronagraphs adapted to complicated pupils are highly sensitive to tip/tilt aberrations.²⁶ The ‘leaked’ stellar flux that ends up in the image plane due to tip/tilt is the limiting factor for effective starlight suppression for the PAVC.²⁷ The angular size of on-axis stars will pose a similar problem for vortex coronagraphs designed for future telescopes with large primary mirrors.²⁸ This is the case even for vortex phase masks with topological charges ≥ 4 , which are robust to low order aberrations with unobscured pupils.^{28,29}

Since the distortion imposed by the central obscuration appears to make the dominant contribution to the leaked flux, making the PAVC insensitive to flux at small angular offsets from the position of the on-axis star is an appealing avenue for addressing the limitation to coronagraphic performance imposed by this flux. In this paper, we explore methods for designing apodizing filters that render the PAVC robust to small angular offsets. By adding constraints to the linear program used to optimize PAVCs apodized with a greyscale filter, we demonstrate that the PAVC may be made robust to offsets as large as $0.01 - 0.1 \lambda/D$ for central obstructions the size of those in the LUVOIR or WFIRST pupils at the expense of throughput. We also demonstrate that PAVCs with topological charge ≥ 4 can be designed with the same sensitivity to small angular offset as vortex coronagraphs of corresponding charge on unobscured pupils. These modifications to the PAVC lay the groundwork for designing vortex coronagraphs for complicated pupils that are robust to both tip/tilt aberrations and stellar angular size.

2. GREYSCALE PAVC DESIGN

2.1 Vortex Topological Charge

The defining feature of a vortex coronagraph is that it uses a vortex phase mask in the focal plane to redistribute on-axis starlight out the telescope pupil for unobstructed, circular pupils. A vortex phase mask impose a phase ramp $e^{ic\theta}$ on the electric field propagating through it, where θ is the angle in polar coordinates centered on the center of the mask and c is the topological charge. If c is an even integer, the vortex will re-arrange light from a uniform disk in the pupil plane to ring around the disk.³⁰ If the pupil is a uniform disk, the end result is that on-axis starlight is entirely rejected, while for a pupil with a central obstruction, two concentric rings are formed, and the vortex coronagraph must be modified to suppress the starlight in the inner disk.^{19,31,32}

The charge of the vortex determines both the coronagraph’s IWA and sensitivity to low-order aberrations. As the charge increases, so does the IWA (in this case defined to be the angular separation where off-axis source throughput is 0.5 the maximum throughput at large separations), from $\sim 1.0 \lambda/D$ for a charge 2 vortex to $\sim 3.5 \lambda/D$ for a charge 8. However, increasing the charge of the vortex will also decrease the sensitivity of the vortex coronagraph to low-order aberrations.^{28,29} A charge 4 or 6 vortex coronagraph on a circular pupil offers a good compromise between IWA and sensitivity to tip/tilt and stellar angular size.²⁸

Unfortunately, for complicated pupil geometries with central obstructions and spiders, vortex coronagraphs of all charges are more sensitive to tip/tilt and finite stellar angular size.²⁶ In an example PAVC6+ACAD-OSM coronagraph described in Mazoyer et al. *in prep.*,²⁷ the leaked flux from a tip/tilt offset of $0.01 \lambda/D$ limited starlight suppression to 10^{-9} in the image plane, and was driven primarily by the central obstruction.

2.2 Overview of the PAVC

The PAVC uses analytically derived pupil apodizations to null on-axis stellar flux in the Lyot plane of a vortex coronagraph for pupils with central obscurations. These apodizations can be produced either by a greyscale apodizing filter or a pair of shaped mirrors. In the present discussion, we limit our attention to the greyscale apodizing PAVC, which is depicted in Figure 1.

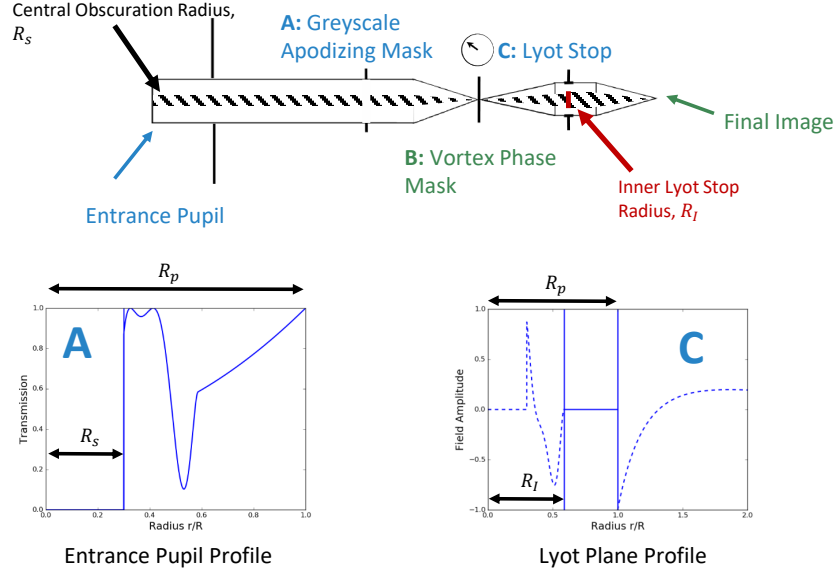


Figure 1. Overview of the greyscale apodized PAVC from Paper I (Figure 1 in Paper I). There are three stages in the PAVC, the pupil-plane greyscale apodizing filter (Stage A), the vortex phase mask (Stage B), and the Lyot stop (Stage C). The inset in the lower left provides an example PAVC4 apodization function produced by the filter at stage A. At Stage C, the Lyot stop blocks all light at $r < R_I$ and $r > R_P$, resulting in complete nulling of the on-axis source.

The apodization function produced by the PAVC greyscale apodizer, $A(r)$, is the piecewise polynomial,

$$A(r) = \begin{cases} \sum_{n=0}^N a_n r^n, & \text{if } R_S < r \leq R_I, \\ \sum_{n=0}^N a_n r^n + b_n r^n, & \text{if } R_I < r \leq R_P, \end{cases} \quad (1)$$

where R_S is the radius of the central obscuration imposed by the secondary mirror, R_P is the radius of the primary mirror, and R_I is the radius of the inner Lyot stop (see Stage C in Figure 1). N is the order of the piecewise polynomial used to parameterize $A(r)$ —throughout this paper we use $N = 16$.

When on-axis starlight propagates through the PAVC setup shown in Figure 1 the electric field in the Lyot plane may be described analytically. This analytical description allows combinations of the values of A_n and B_n in Equation 1 to be found that produce zero electric field in the Lyot plane between R_I and R_P . The inner Lyot stop at Stage C in Figure 1 blocks the field at $r < R_I$, so the on-axis starlight is entirely suppressed.¹⁸

For a given value of R_I (as long as $R_I > R_S$), the values of A_n and B_n may be solved by a linear program that maximizes transmission through the greyscale filter in Stage A in Figure 1,

$$T = \int_{R_I}^{R_P} A(r) r dr, \quad (2)$$

subject to linear constraints that ensure the Lyot field is zero between R_I and R_P . Additional constraints may be added to ensure that e.g. $A(r)$ is smooth. For the greyscale PAVC designs discussed in this paper, the only constraints from Paper I that we care about are those that ensure on-axis starlight is completely suppressed.

Analytical expressions for the Lyot plane electric field of a PAVC for topological charges 2-6 are given in Equations 7-9 in Paper I. These expressions are used to find the linear constraints that null the Lyot plane field,

given in Equations 11-13 in Paper I. In this paper, we discuss tip/tilt robust versions of the PAVC4, PAVC6, and PAVC8. Therefore, we present constraints that ensure a PAVC8 will completely block on-axis starlight.

$V_8[A(r)]$ is defined to be the operator that maps the apodized pupil (plane A in Figure 1 of a vortex coronagraph with topological charge 8 to the electric field in the Lyot plane (plane C) (V_8 is defined analogous to V_2 , V_4 , and V_6 in Paper I). For each term r^n of $A(r)$ in Equation 1, we get

$$V_8[r^n] = \frac{n(n-2)(n-4)(n-6)}{(n+2)(n+4)(n+6)(n+8)}r^n - \frac{8}{n+2}R_X^{n+2}r^{-2} + \frac{120}{n+4}R_X^{n+4}r^{-4} - \frac{360}{n+6}R_X^{n+6}r^{-6} + \frac{280}{n+8}R_X^{n+8}r^{-8}, \quad (3)$$

where $R_X = R_S$ for the ' A_n ' terms in Equation 1, and $R_X = R_I$ for the ' B_n ' terms. Equation 3 implies that $V_8[A(r)] = 0$ in the region $R_I \leq r \leq R_P$ if the following constraints are obeyed:

$$\sum_{n=0}^N \left(-\frac{8R_S^{n+2}}{n+2}A_n - \frac{8R_I^{n+2}}{n+2}B_n \right) = 0, \quad (4a)$$

$$\sum_{n=0}^N \left(\frac{120R_S^{n+4}}{n+4}A_n + \frac{120R_I^{n+4}}{n+4}B_n \right) = 0, \quad (4b)$$

$$\sum_{n=0}^N \left(-\frac{360R_S^{n+6}}{n+6}A_n - \frac{360R_I^{n+6}}{n+6}B_n \right) = 0, \quad (4c)$$

$$\sum_{n=0}^N \left(\frac{280R_S^{n+8}}{n+8}A_n + \frac{280R_I^{n+8}}{n+8}B_n \right) = 0, \quad (4d)$$

$$A_n + B_n = 0, \text{ if } n \neq (0, 2, 4, 6). \quad (4e)$$

2.3 Tip/Tilt Robustness

In order to address the issue of tip/tilt robustness, we derive new constraints that can be added to the linear program used to optimize the greyscale PAVC. We start by calculating the approximate Lyot plane electric field obtained when the star observed by the PAVC is offset from the on-axis position by a small angle s . We then show this expression can be used to define constraints that can be used to optimize versions of the PAVC that permit leaked on-axis stellar fluxes of $\leq 10^{-10}$ relative to the peak flux of the stellar point spread function (PSF) for offsets as large as s .

For a telescope with a central obstruction of radius R_S and a PAVC with apodization function $A(r)$, the electric field in the pupil plane of a source at $(s, 0)$ in polar coordinates is

$$E_{pup} = \begin{cases} A(r) e^{i\pi \frac{\lambda}{\lambda_0} sr \cos \theta}, & \text{if } R_S \leq r \leq R_P \\ 0, & \text{if } r < R_S, r > R_P \end{cases} \quad (5)$$

where λ_0 is the central wavelength of the broadband filter used to measure photometry in the coronagraphic image, λ is the wavelength of the electric field, and (r, θ) are the polar coordinates of the pupil plane centered on the axis of the telescope. Since the PAVC is circularly symmetric, we can assume the source is at $\theta = 0$ without loss of generality. For an individual component of $A(r)$, the field is

$$E_{pup}^n = \begin{cases} A_n r^n e^{i\pi \frac{\lambda}{\lambda_0} sr \cos \theta}, & \text{if } R_S \leq r \leq R_P \\ 0, & \text{if } r < R_S, r > R_P \end{cases} \quad (6)$$

For the B_n components, R_S is replaced by R_I .

Equation 6 may be expanded as

$$E_{pup}^n = A_n \sum_{j=0}^{\infty} \sum_{k=0}^j C_{jk} s^j r^{j+n} e^{i(j-2k)\theta} \quad (7)$$

where

$$C_{jk} \equiv \left(\frac{i\pi \frac{\lambda}{\lambda_0}}{2} \right)^j \frac{1}{j!} \binom{j}{k}. \quad (8)$$

As long as $s \leq 0.1 \lambda_0/D$, for the purposes of keeping the leaked flux below 10^{-10} in units normalized to the peak of the stellar PSF, it is sufficient to only consider terms in the expansion in Equation 7 up to $j = 5$.

The propagated electric field for a source with offset s can be expanded analytically in the Lyot plane. For a charge 4 PAVC, for each term r^n of $A(r)$ the analytical expansion of the Lyot field is,

$$\begin{aligned} E_{Lyot}^n &= e^{i4\theta} V_4[r^n] + C_{10}s e^{i5\theta} \left[\frac{n(n-2)}{(n+4)(n+6)} r^{n+1} - \frac{12}{n+4} R_X^{n+4} r^{-3} + \frac{24}{n+6} R_X^{n+6} r^{-5} \right] \\ &\quad + C_{11}s e^{i3\theta} \left[\frac{n}{n+4} r^{n+1} + \frac{4}{n+4} R_X^{n+4} r^{-3} \right] \\ &\quad + C_{20}s^2 e^{i6\theta} \left[\frac{n(n-2)}{(n+6)(n+8)} r^{n+2} - \frac{8}{n+6} R_X^{n+6} r^{-4} + \frac{40}{n+8} R_X^{n+8} r^{-6} \right] \\ &\quad + C_{21}s^2 e^{i4\theta} \left[\frac{n(n+2)}{(n+4)(n+6)} r^{n+2} - \frac{4}{n+4} R_X^{n+4} r^{-2} + \frac{12}{n+6} R_X^{n+6} r^{-4} \right] \\ &\quad + C_{22}s^2 e^{i2\theta} r^{n+2} + \mathcal{O}(s^3), \end{aligned} \quad (9)$$

where as before, $R_X = R_S$ for the A_n components of $A(r)$ and $R_X = R_I$ for the B_n components. $V_4[r^n]$ is the charge 4 vortex operator described in Paper I, and $e^{i4\theta} V_4[r^n]$ is the Lyot field if $s = 0$. For brevity and readability, we only expand E_{Lyot}^n to order s^2 . For a charge 6 PAVC the field is,

$$\begin{aligned} E_{Lyot}^n &= e^{i6\theta} V_6[r^n] + C_{10}s e^{i7\theta} \left[-\frac{n(n-2)(n-4)}{(n+4)(n+6)(n+8)} r^{n+1} - \frac{24}{n+4} R_X^{n+4} r^{-3} + \frac{120}{n+6} R_X^{n+6} r^{-5} - \frac{120}{n+8} R_I^{n+8} r^{-7} \right] \\ &\quad + C_{11}s e^{i5\theta} \left[-\frac{n(n-2)}{(n+4)(n+6)} r^{n+1} + \frac{12}{n+4} R_X^{n+4} r^{-2} - \frac{24}{n+6} R_X^{n+6} r^{-5} \right] \\ &\quad + C_{20}s^2 e^{i8\theta} \left[-\frac{n(n-2)(n-4)}{(n+6)(n+8)(n+10)} r^{n+2} - \frac{60}{n+6} R_X^{n+6} r^{-4} + \frac{240}{n+8} R_X^{n+8} r^{-6} - \frac{210}{n+10} R_X^{n+10} r^{-8} \right] \\ &\quad + C_{21}s^2 e^{i6\theta} \left[-\frac{n(n-2)(n+2)}{(n+4)(n+6)(n+8)} r^{n+2} - \frac{6}{n+4} R_X^{n+4} r^{-2} + \frac{48}{n+6} R_X^{n+6} r^{-4} - \frac{60}{n+8} R_X^{n+8} r^{-6} \right] \\ &\quad + C_{22}s^2 e^{i4\theta} \left[-\frac{n}{n+6} r^{n+2} - \frac{6}{n+6} R_X^{n+6} r^{-4} \right] \\ &\quad + C_{30}s^3 e^{i9\theta} \left[-\frac{n(n-2)(n-4)}{(n+8)(n+10)(n+12)} r^{n+3} - \frac{120}{n+8} R_X^{n+8} r^{-5} + \frac{420}{n+10} R_X^{n+10} r^{-7} - \frac{336}{n+12} R_X^{n+12} r^{-9} \right] \\ &\quad + C_{31}s^3 e^{i7\theta} \left[-\frac{n(n-2)(n+2)}{(n+6)(n+8)(n+10)} r^{n+3} - \frac{24}{n+6} R_X^{n+6} r^{-3} + \frac{120}{n+8} R_X^{n+8} r^{-5} - \frac{120}{n+10} R_X^{n+10} r^{-7} \right] \\ &\quad + C_{32}s^3 e^{i5\theta} \left[-\frac{n(n+2)}{(n+6)(n+8)} r^{n+3} + \frac{12}{n+6} R_X^{n+6} r^{-3} - \frac{24}{n+8} R_X^{n+8} r^{-5} \right] - C_{33}s^3 e^{i3\theta} r^{n+3} + \mathcal{O}(s^4). \end{aligned} \quad (10)$$

For a charge 8 PAVC, similar expressions may be written, which we do not include for brevity.

These expressions can be used to either to constrain the leaked flux from a small offset to be $\leq 10^{-10}$, or can be used to design PAVCs that have the same sensitivity to small angular offsets as vortex coronagraphs with uniform, circular pupils. For the latter case, it is necessary to constrain the leading orders of s in the total Lyot field, E_{Lyot} , to be 0. The sensitivity of a vortex coronagraph to a small angular offset s is $\propto s^c$, where c is the vortex topological charge. Therefore, in order find a PAVC4 with the same offset sensitivity as a charge 4 vortex, it is necessary to impose the following constraints on A_n and B_n in $A(r)$:

$$\sum_{n=0}^N (R_S^{n+6} A_n + R_I^{n+6} B_n) = 0, \quad (11a)$$

$$\sum_{n=0}^N (R_S^{n+4} A_n + R_I^{n+4} B_n) = 0, \quad (11b)$$

$$A_n + B_n = 0, \text{ if } n \neq 0. \quad (11c)$$

$$\int_{R_I}^{R_P} \sum_{n=0}^N [E_{Lyot}^n(s^2, R_S) A_n + E_{Lyot}^n(s^2, R_I) B_n] r dr \leq \frac{\pi^2}{\sqrt{32}}, \quad (11d)$$

where $E_{Lyot}^n(s^2, R_X)$ is the sum of all the s^2 terms in Equation 9. The three first constraints ensures that the leading term in the electric field amplitude in the Lyot plane goes as s^2 , therefore that the leading term in the flux is s^4 . The final constraint ensures that the leading term in the expression for the PAVC E_{Lyot} is \leq the leading term for the unobscured vortex E_{Lyot} , which was calculated in Jenkins et al. 2008.²⁹ For the charge 6 PAVC, the equivalent constraints are:

$$\sum_{n=0}^N (R_S^{n+10} A_n + R_I^{n+10} B_n) = 0, \quad (12a)$$

$$\sum_{n=0}^N (R_S^{n+8} A_n + R_I^{n+8} B_n) = 0, \quad (12b)$$

$$\sum_{n=0}^N (R_S^{n+6} A_n + R_I^{n+6} B_n) = 0, \quad (12c)$$

$$\sum_{n=0}^N (R_S^{n+4} A_n + R_I^{n+4} B_n) = 0, \quad (12d)$$

$$A_n + B_n = 0, \text{ if } n \neq 0. \quad (12e)$$

$$\int_{R_I}^{R_P} \sum_{n=0}^N [E_{Lyot}^n(s^3, R_S) A_n + E_{Lyot}^n(s^3, R_I) B_n] r dr \leq \frac{\pi^3}{\sqrt{240}}. \quad (12f)$$

While these expressions will produce robust PAVC designs with sensitivities matching unobscured vortex coronagraphs, we are mostly interested in ensuring that the effective starlight suppression of a PAVC in the presence of tip/tilt or stellar angular size is at least 10^{-10} . In order to constrain leaked flux to $\leq 10^{-10}$, the expressions for E_{Lyot}^n are propagated to the image plane. By propagating into the image plane, we can constrain the leaked flux between a desired IWA and outer working angle (OWA) (in this case, IWA and OWA are defined to be the radial boundaries of the dark hole in the image plane), which allows us to impose weaker constraints on $A(r)$ than would be necessary to constrain the leaked flux in the Lyot plane. Furthermore, since we have already calculated the electric field in the Lyot plane, we were able to avoid the numerical artifacts that occur when numerically propagating a beam through a vortex filter in the focal plane.³³ E_{Lyot}^n is separable, and so can be written as

$$E_{Lyot}^n = \mathcal{R}_{Lyot}^n(r, R_X) e^{im\theta}, \quad (13)$$

where $\mathcal{R}_{Lyot}^n(r, R_X)$ captures the radial dependence of the field in the Lyot plane. For each term r^n in $A(r)$, the corresponding field in the image plane is:

$$E_{Image}^n(k, \theta, R_X) \equiv \pi e^{im\theta} \int_{R_I}^{R_P} \mathcal{R}_{Lyot}^n(r, R_X) J_m(\pi kr) r dr. \quad (14)$$

We do not report the closed form for this expression, since it is not useful for this analysis.

In order to ensure that suppression of leaked flux is 10^{-10} between the IWA and OWA, we constrain both the real and imaginary components of the electric field in the image plane. The constraints are

$$-10^{-5} \leq \frac{1}{f_{Peak}} \sum_{n=0}^N [A_n \operatorname{Re}(E_{Image}^n(k, \theta, R_S)) + B_n \operatorname{Re}(E_{Image}^n(k, \theta, R_I))] \leq 10^{-5}, \quad (15a)$$

$$-10^{-5} \leq \frac{1}{f_{Peak}} \sum_{n=0}^N [A_n \text{Im}(E_{Image}^n(k, \theta, R_S)) + B_n \text{Im}(E_{Image}^n(k, \theta, R_I))] \leq 10^{-5}, \quad (15b)$$

where f_{Peak} is the peak flux from the on-axis star observed without a coronagraph. In principle these constraints are slightly too lax, since a coronagraph with leaked flux limiting starlight suppression to 1.4×10^{-10} would still meet them. However, making the linear constraints more stringent would result in missing possible solutions to the problem of robust PAVC design. As shown in the results, we find that the actual tip/tilt robust designs we produce have a peak normalized leaked flux of $< 10^{-10}$. In order to measure broadband light, we imposed five sets of constraints for wavelengths spaced evenly between $0.85 \lambda_0/D$ and $1.15 \lambda_0/D$.

2.4 Modifications to the PAVC Algorithm

In this paper we made two changes to the algorithm used in Paper I to optimize the PAVC. First, while we continue to use transmission as the figure of merit for optimizing $A(r)$ for each combination of R_S and R_I , we now choose the value of R_I for a given R_S that maximizes the E.E. throughput at a desired off-axis source position. For the coronagraphs designed for a LUVOIR-like secondary mirror, we choose $3 \lambda/D$ as the desired off-axis position, and for the WFIRST-like secondary, we choose $5 \lambda/D$.

Second, we also try oversizing the inner and outer Lyot stops. A PAVC will still exactly null the Lyot plane electric if the radius of the inner Lyot stop is $> R_I$. Adding an outer Lyot stop will not affect Lyot plane nulling either. We find that incorporating oversized Lyot stops will improve leaked flux suppression only for relatively large values of s (i.e. $s \sim 0.1 \lambda/D$).

3. RESULTS

We present two sets of results for PAVCs designed to incorporate robustness to small angular offsets. First, we discuss designing a charge 4, 6, or 8 PAVC to have the same sensitivity to small angular offsets as a charge 4, 6, or 8 vortex coronagraph with an unobscured, circular pupil. The T.E. throughput of these designs fares poorly for large central obstructions, so we focus most of our attention on designs that suppress leaked flux in between the IWA and OWA in the image plane. We explore the relationship between E.E. throughput and the maximum angular offset s the coronagraph is robust against for a telescope with a circular secondary mirror of radius $R_S = 0.17R_P$ and $R_S = 0.36R_P$. These central obstruction sizes were selected to reflect the configurations of the LUVOIR and WFIRST telescopes, respectively.^{1,2}

3.1 Matching Unobscured Vortex Tip/Tilt Sensitivity

Apodizing masks were computed for the charge 4 and 6 PAVC that match the ‘native’ small angular offset sensitivity of the vortex coronagraph. For the PAVC4, the leaked flux goes as s^4 to first order, and for the PAVC6, the flux goes as s^6 . The T.E. throughput of these designs as a function of R_S are shown in Figure 2. Examples for $R_S = 0.1R_P$ are shown in Figure 3.

Designs matching native vortex coronagraph sensitivity are similar to the Ring Apodized Vortex Coronagraph (RAVC), which employs a pupil apodization function consisting of concentric rings of uniform transmission.³¹ This is because the constraints listed in Equations 11 and 12 required to achieve this level of sensitivity require that $A(r) = A_n + B_n$ in the region $R_I \leq r \leq R_P$. The part of the pupil plane that is not blocked by the inner Lyot stop is therefore a ring of uniform transmission. Like the RAVC, these robust designs have rapidly diminishing throughput performance as a function both of R_S and of topological charge. $A(r)$ for the designs presented in this section is subject to a greater number of constraints than the equivalent RAVC apodization function, and as a result the T.E. performance of these designs degrades more quickly than the RAVC as R_S increases.

Unobscured Vortex- Matching PAVC Throughput

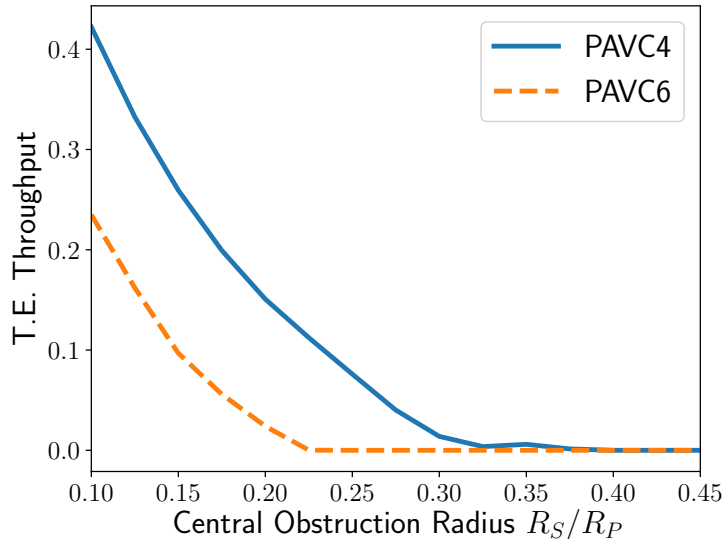


Figure 2. Throughput of the optimally robust PAVC4 and PAVC6 as a function of central obstruction radius, R_S . The T.E. throughput of a PAVC4 optimized to match the tip/tilt sensitivity of an unobscured charge 4 vortex coronagraph is shown as the blue solid line, and the T.E. throughput of a PAVC6 optimized to match the tip/tilt sensitivity of an unobscured charge 6 vortex is shown as the orange dashed line. To leading order, the leaked flux from a source as small angular offset goes as s^4 for the PAVC4 and as s^6 for the PAVC6.

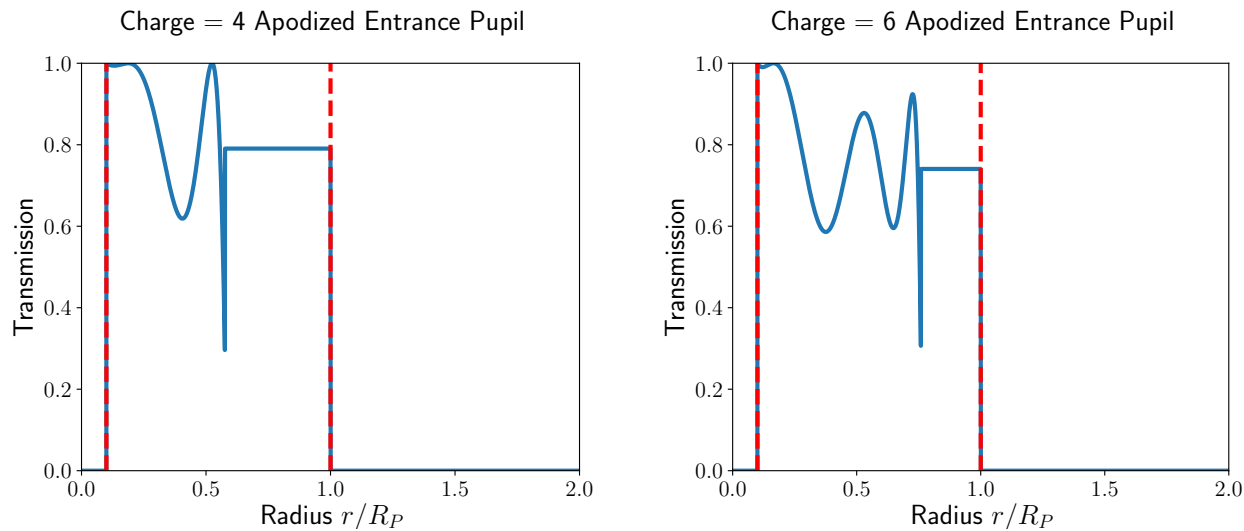


Figure 3. $A(r)$ for a PAVC4 (left) and PAVC6 (right) optimized to match the tip/tilt sensitivity of an unobscured vortex coronagraph of charge 4 and 6, respectively. Solid blue curves denote the apodization function, and dashed red lines denote R_S and R_P .

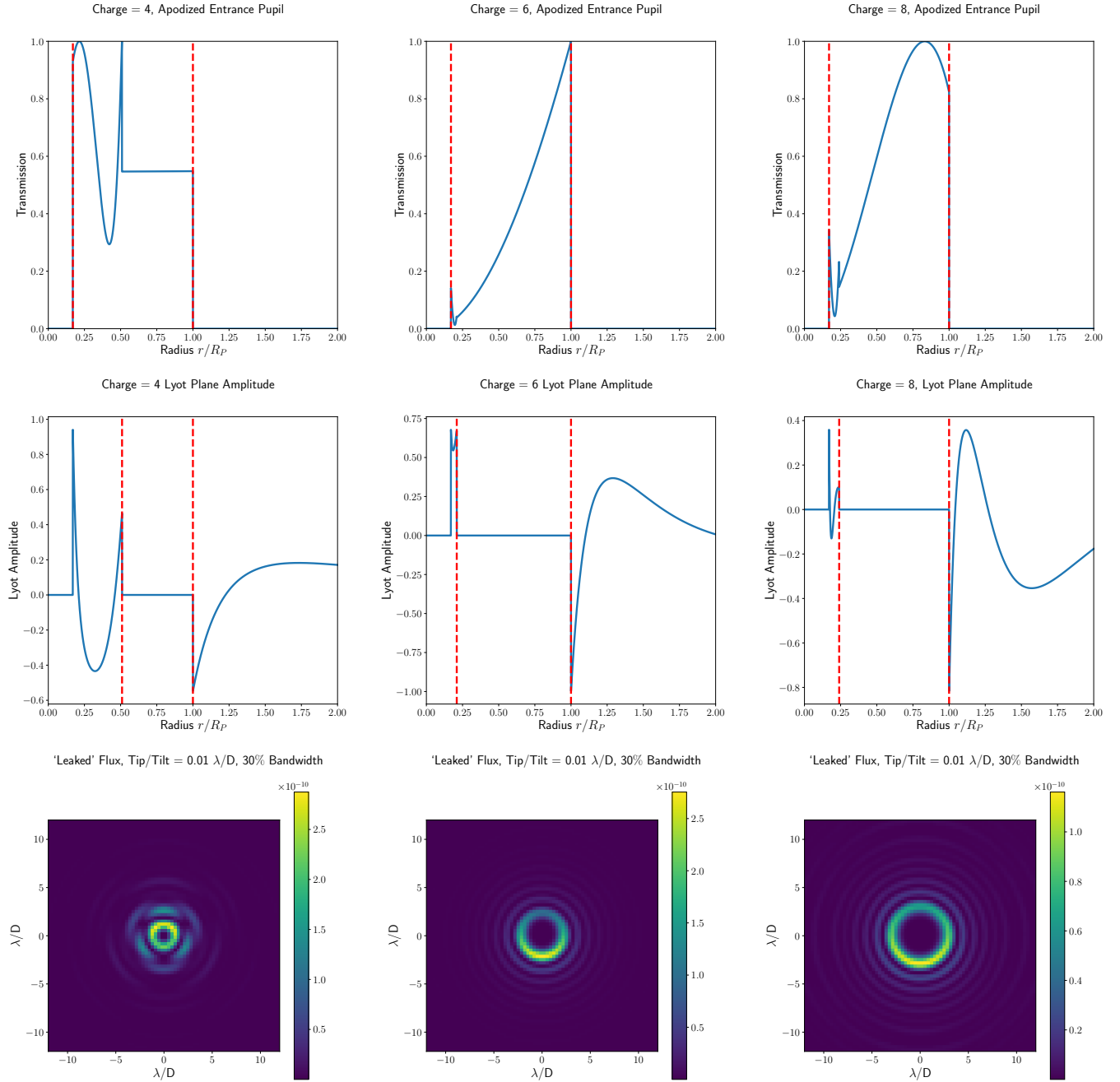


Figure 4. *Top Row:* Apodizations for PAVC4, PAVC6, and PAVC8 coronagraphs with a normalized flux leak of $< 10^{-10}$ given an on-axis source offset of $0.01 \lambda/D$. Solid blue curves denote the apodization function, and dashed red lines denote R_S and R_P . *Middle Row:* Profiles of the ‘ideal’ on-axis source Lyot plane electric field amplitude are shown in the absence of offset. For point sources that do not experience tip/tilt offsets, the PAVC cancels out the electric field amplitude in the Lyot plane entirely. The red dashed lines in these plots show R_I and R_P . Light at radii $< R_I$ and $> R_P$ is blocked by the Lyot stop. *Bottom Row:* Image plane fluxes of on-axis sources offset by $s = 0.01 \lambda/D$ in 30% bandwidth light. The coronagraphs were optimized to form a dark hole in the region $3 \lambda/D < s < 12 \lambda/D$.

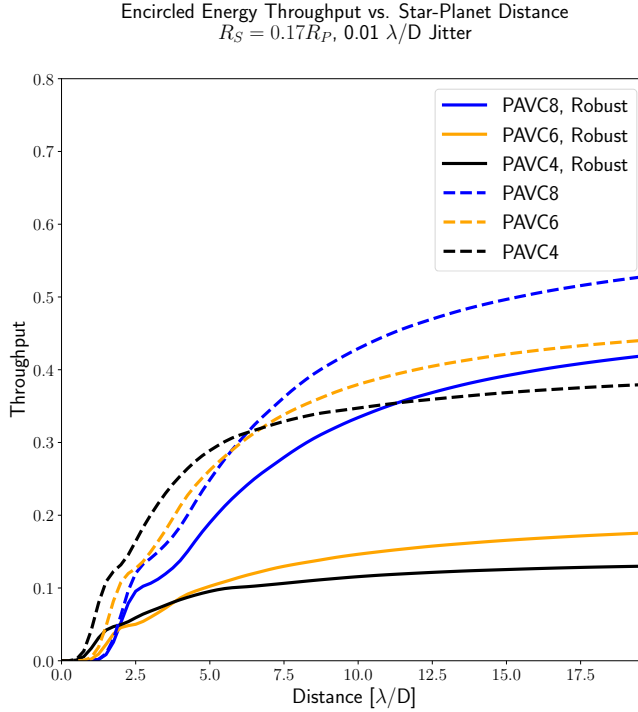


Figure 5. E.E. throughput of an off-axis source as a function of angular separation between the source and on-axis star. The solid blue line shows throughput as a function of separation for a PAVC8 robust to offsets of 0.01 λ/D , the orange line shows the same for the PAVC6 and the black line shows the same for the PAVC4. Dashed lines depict the same curves, but for PAVC solutions calculated without constraints to ensure robustness to tip/tilt offsets.

3.2 LUVOIR Secondary Mirror

We present robust PAVC4, PAVC6, and PAVC8 designs for a telescope with $R_S = 0.17R_P$. In Figure 4, we present apodizations that suppress leaked flux from an on-axis source with a small angular offset as large as 0.01 λ/D in a region between 3-12 λ/D in the image plane with 30% broadband light. We show $A(r)$, the Lyot plane field for a perfectly on-axis source (i.e. a perfect point source with no tip/tilt) and the final dark hole.

E.E. and T.E. throughputs as a function of angular separation between an exoplanet and the on-axis star for these instruments are shown in Figures 5 and 6 for PAVC designs robust to offsets of 0.01 λ/D . Compared to the PAVC designs that assume no aberrations, the 0.01 λ/D -robust PAVC4 experiences a factor of ~ 3.5 reduction in E.E. throughput at large separations from the on-axis star and a similar reduction at a separation of 3 λ/D . For the PAVC6 E.E. throughput degradation is slightly worse at both large separations and at 3 λ/D . Meanwhile, the PAVC8 design we present here performs about as well as the non-robust PAVC6, suggesting the PAVC8 may be an appealing option for a tip/tilt robust coronagraph on LUVOIR.

In Figure 7, we show the same results for the PAVC6 and PAVC8 that suppresses leaked flux from offsets as large as 0.1 λ/D . For tip/tilt offsets of this magnitude, only the PAVC8 provides meaningful levels of throughput, achieving $\sim 25\%$ T.E. throughput and $\sim 15\%$ E.E. throughput at large angular separations.

3.3 WFIRST Secondary Mirror

We now discuss robust PAVC designs for a telescope with $R_S = 0.36R_P$, which is comparable to the WFIRST secondary mirror radius. We present apodizations and dark holes for instruments that suppress sources at small offsets $s \leq 0.01\lambda/D$ in a region between 5-12 λ/D in the image plane with 30% broadband light in Figure 8. E.E. and T.E. throughput as a function of source angular separation in Figures 9 and 10.

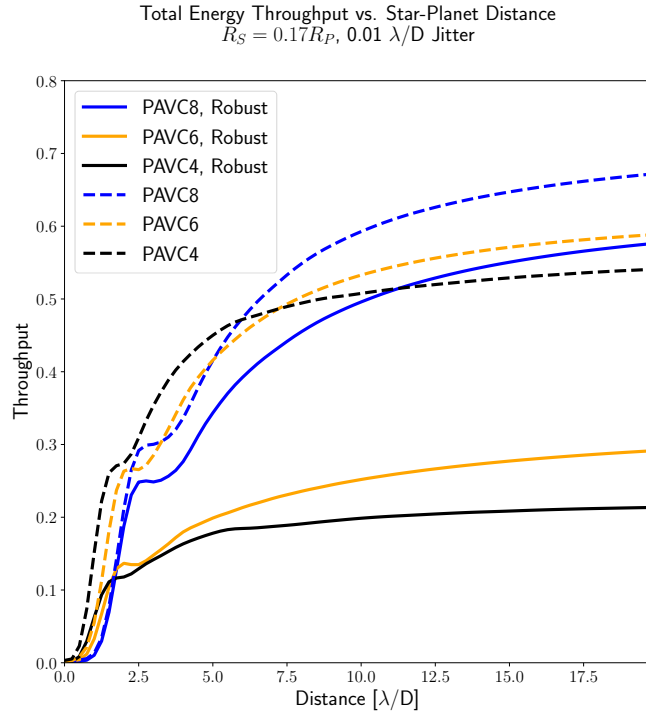


Figure 6. T.E. throughput of an off-axis source as a function of angular separation between the source and on-axis star. This figure shows the same material as Figure 5, except for T.E. throughput.

Unlike the LUVOIR-like case, while the PAVC8 provides higher E.E. throughput at large angular separations, it is outperformed by the PAVC6 near $5 \lambda/D$. This discrepancy results from two competing factors driving the relative performance of the PAVC6 and PAVC8. On the one hand, the transmission through the apodized pupil of the PAVC increases as the charge of the vortex increases.¹⁸ For any given R_S , the PAVC8 will have a higher transmission through the pupil than the PAVC6. However, as discussed above, the IWA of the vortex focal plane mask itself increases as the charge increases. We also find that the E.E. throughput of a charge 8 vortex coronagraph at a set distance from the on-axis source degrades more rapidly than the E.E. throughput of a charge 6 vortex coronagraph as a function of R_S and as a function of R_I . In the case of a WFIRST-like secondary mirror, at small separations, the second effect wins out over the first, resulting in the PAVC6 having superior E.E. throughput compared to the PAVC8.

4. DISCUSSION

Modifying the linear constraints used to design the PAVC is successful at making the PAVC robust to small angular offsets between the position of the on-axis star and the on-axis position of the telescope. These relatively simple constraints significantly reduce the sensitivity of the PAVC to small angular offsets, although they do so at the expense of throughput. Figure 11 shows the trade-off between E.E. throughput at small angular separations and the maximum offset for which the PAVC suppresses flux to 10^{-10} for a LUVOIR-like and WFIRST-like secondary mirror. For the LUVOIR-like case, for a planet orbiting its star at a distance of $3\lambda/D$ the PAVC4 provides the best E.E. throughput in the absence of significant tip/tilt offsets, owing to the small IWA of the charge 4 vortex. However, across three orders of magnitude in offset, we see that the E.E. throughput of the PAVC8 is reduced by a factor of ~ 2 , the PAVC6 by a factor of ~ 7 , and the performance of the PAVC4 degrades completely. Meanwhile, for the WFIRST-like case, the PAVC6 always provides the best performance—the smaller charge 6 vortex IWA beats out the charge 8 vortex, while the PAVC6 apodization provides substantially higher transmission than the PAVC4 apodization for a large central obscuration.

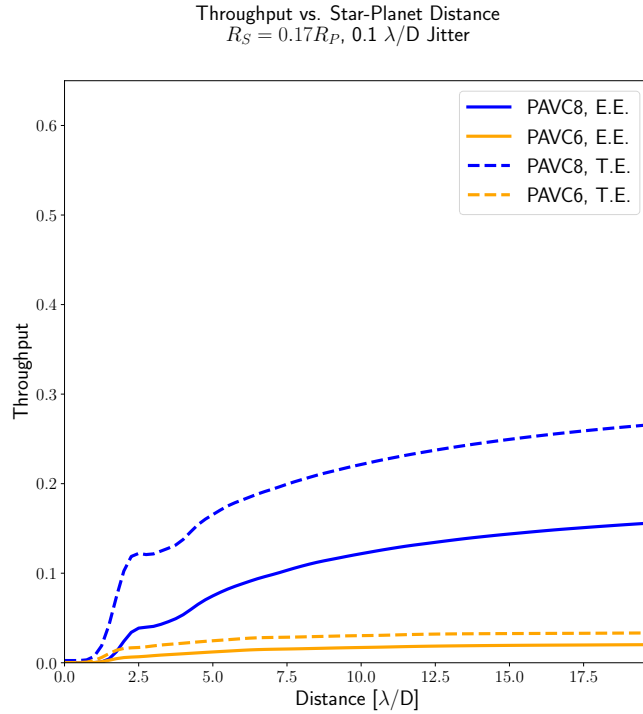


Figure 7. E.E. and T.E. throughput of an off-axis source vs. separation for versions of the PAVC6 and PAVC8 optimized to be robust to offsets of $0.1 \lambda/D$. E.E. throughputs are shown as solid lines, T.E. throughputs are shown as dashed lines.

The robust PAVC designs we discuss in this paper provide proof of concept for apodized vortex coronagraphs that can provide ideal on-axis starlight suppression and insensitivity to reasonable large tip/tilt offsets. While we have investigated some of the available parameter space by modifying $A(r)$ on a PAVC using an apodizing filter and by exploring use of oversized inner and outer Lyot stops, we are still exploring several possible options for improving the trade-off between offset sensitivity and throughput. Possible avenues including adding a central spot to the focal plane mask and modifying versions of the PAVC that use shaped mirrors to apodize the pupil may improve coronagraphic performance substantially.

A PAVC that suppresses flux at the 10^{-10} level for sources at small angular offsets $\leq s$ will also suppress leaked flux from a star with an angular radius slightly larger than s . However, it will not suppress leaked flux from a star substantially larger than s . For stars with radii approaching $1 \lambda/D$, it will be necessary to improve on the robustness constraints discussed in this paper.

While the robust PAVC designs we present only address leaked flux induced by a circularly symmetrical central obstruction, we can couple the PAVC with procedures to mitigate the impact of spiders on starlight suppression. Mazoyer et al. *in prep.*²⁷ explicitly couples ACAD-OSM with several techniques to correct for the central obstruction including a non-robust PAVC, and found that the limiting factor affecting tip/tilt robustness in the combined designs was the sensitivity of the technique used to address the central obstruction. Therefore, tip/tilt robust PAVC designs provide a clear path to building robust, high-throughput coronagraphs for arbitrary apertures.

5. CONCLUSIONS

We present linear constraints that can be imposed on the apodization function, $A(r)$, of greyscale filters in order to construct PAVCs that in addition to completely nulling on-axis starlight are highly insensitive to small angular

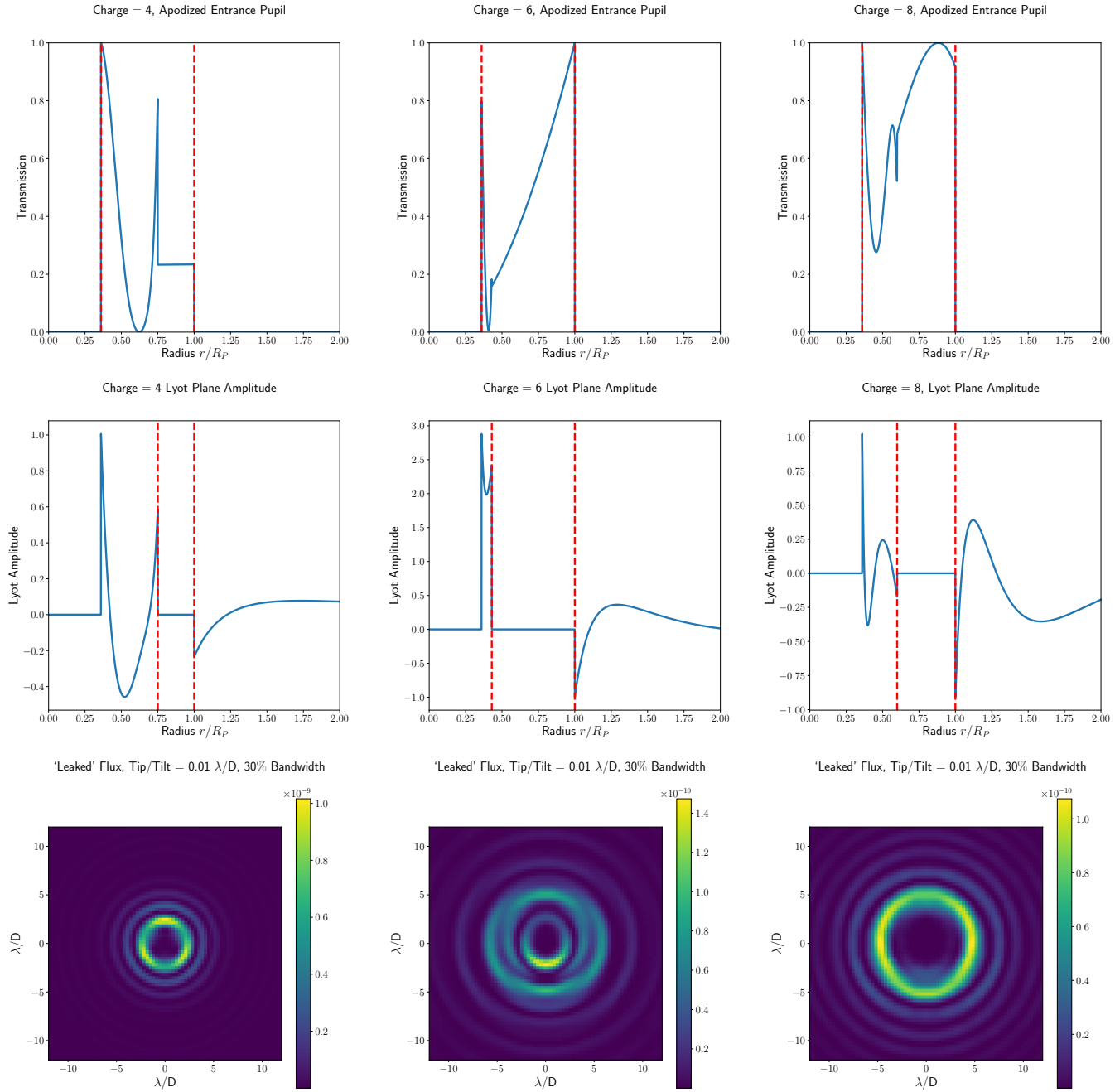


Figure 8. Characteristics of robust PAVC designs computed for a WFIRST-like central obstruction. Results shown are the same as those in Figure 4 with a larger central obstruction with $R_S = 0.36R_P$. The coronagraphs were optimized to form a dark hole in the region $5 \lambda/D < s < 12 \lambda/D$.

Encircled Energy Throughput vs. Star-Planet Distance
 $R_S = 0.36R_P$, 0.01 λ/D Jitter

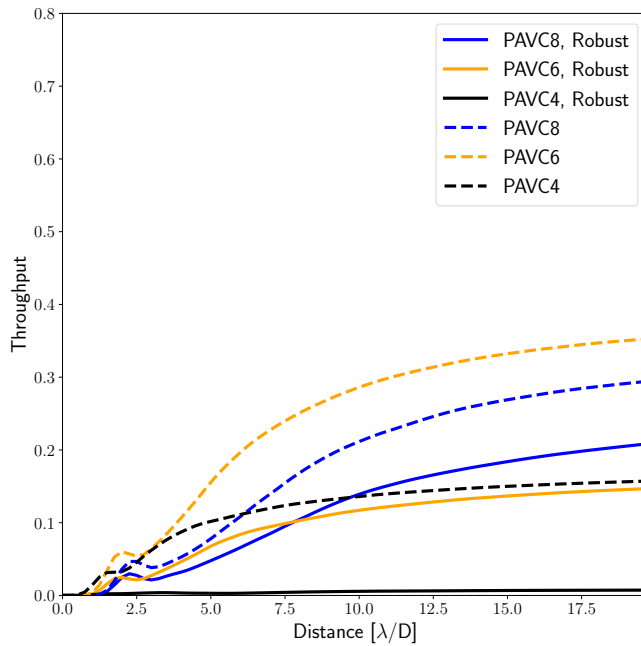


Figure 9. Same as Figure 5, except for designs optimized for $R_S = 0.36R_P$.

Total Energy Throughput vs. Star-Planet Distance
 $R_S = 0.36R_P$, 0.01 λ/D Jitter

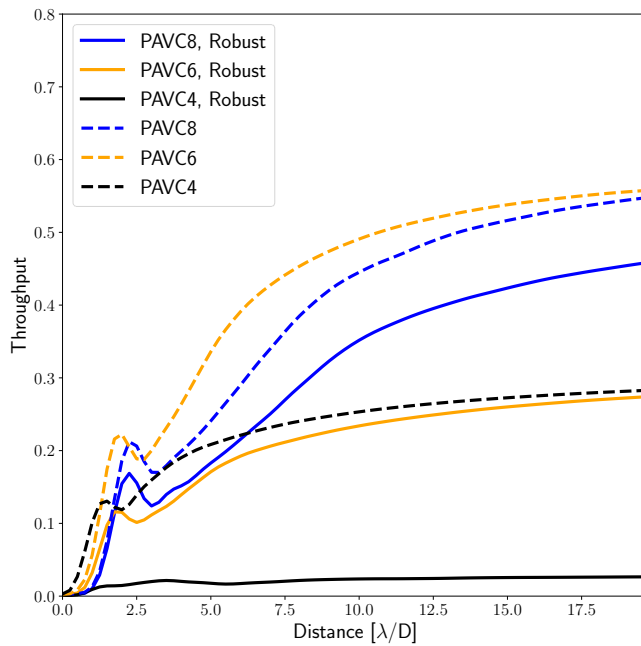


Figure 10. Same as Figure 6, except for designs optimized for $R_S = 0.36R_P$.

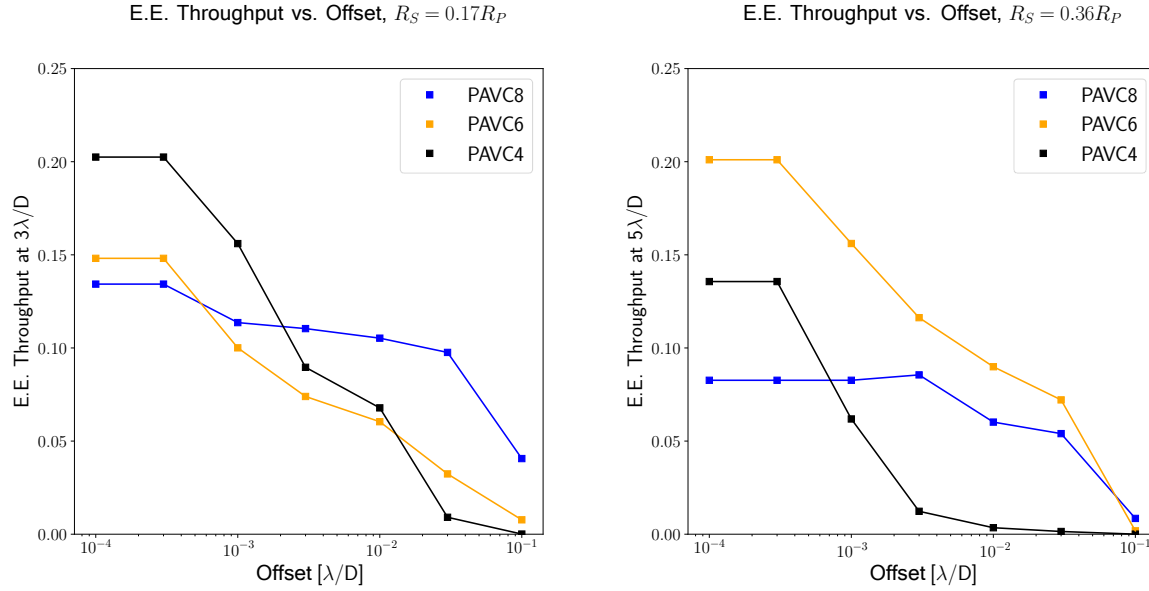


Figure 11. E.E. throughput is shown as a function of magnitude of small jitter offset. The left panel shows the maximum E.E. throughput obtained at $3 \lambda/D$ for PAVC designs optimized for angular offsets between $10^{-4} - 10^{-1} \lambda/D$, for a LUVOIR-like secondary mirror. Optimal throughputs for the PAVC8 are shown in blue, the PAVC6 in orange, and the PAVC4 in black. Individual points show the offsets for which we calculated optimal PAVCs. The right panel shows throughput obtained at $5 \lambda/D$ for a WFIRST-like secondary mirror.

offsets in the position of the on-axis source. By mitigating the leaked flux that results from these small offsets, the resulting PAVC designs are robust to tip/tilt aberrations and to stellar angular scales.

We first investigated adding linear constraints to the PAVC algorithm presented in Paper I that allow us to optimize versions of the PAVC that have the same response to small angular offset as a vortex coronagraph with a uniform, circular pupil. We found that such results do exist, although they have limited throughput performance. We then investigated robust PAVC designs that are capable of suppressing the leaked flux in the image plane to below 10^{-10} in units normalized to the peak flux of the on-axis star PSF. For a central obstruction of radius $R_S = 0.17R_P$, we found that the PAVC8 can be made robust to offsets $\leq 0.01\lambda/D$ while providing E.E. throughputs for off-axis sources comparable to the PAVC6 designs presented in Paper I. We also presented PAVC designs made robust to offsets $\leq 0.1\lambda/D$ at the expense of throughput performance. Finally, we presented PAVC6 and PAVC8 designs for a central obstruction of radius $R_S = 0.36R_P$.

The robust PAVC designs discussed here lay the foundation for designing vortex coronagraphs for complicated pupils that at the same time provide extreme contrasts and robustness to tip/tilt aberrations and stellar angular size. The PAVC therefore addresses a significant hurdle faced by vortex coronagraphs when dealing with complicated pupils with large central obstructions.

ACKNOWLEDGMENTS

This material is partially based upon work carried out under subcontract 1496556 with the Jet Propulsion Laboratory funded by NASA and administered by the California Institute of Technology.

REFERENCES

1. D. Spergel, N. Gehrels, C. Baltay, D. Bennett, J. Breckinridge, M. Donahue, A. Dressler, B. S. Gaudi, T. Greene, O. Guyon, C. Hirata, J. Kalirai, N. J. Kasdin, B. Macintosh, W. Moos, S. Perlmutter, M. Postman, B. Rauscher, J. Rhodes, Y. Wang, D. Weinberg, D. Benford, M. Hudson, W.-S. Jeong, Y. Mellier,

- W. Traub, T. Yamada, P. Capak, J. Colbert, D. Masters, M. Penny, D. Savransky, D. Stern, N. Zimmerman, R. Barry, L. Bartusek, K. Carpenter, E. Cheng, D. Content, F. Dekens, R. Demers, K. Grady, C. Jackson, G. Kuan, J. Kruk, M. Melton, B. Nemati, B. Parvin, I. Poberezhskiy, C. Peddie, J. Ruffa, J. K. Wallace, A. Whipple, E. Wollack, and F. Zhao, "Wide-Field InfrarRed Survey Telescope-Astrophysics Focused Telescope Assets WFIRST-AFTA 2015 Report," *ArXiv e-prints*, Mar. 2015.
2. M. R. Bolcar, K. Balasubramanian, M. Clampin, J. Crooke, L. Feinberg, M. Postman, M. Quijada, B. Rauscher, D. Redding, N. Rioux, S. Shaklan, H. P. Stahl, C. Stahle, and H. Thronson, "Technology development for the Advanced Technology Large Aperture Space Telescope (ATLAST) as a candidate large UV-Optical-Infrared (LUVOIR) surveyor," in *Optics for EUV, X-Ray, and Gamma-Ray Astronomy VII, Society of Photo-Optical Instrumentation Engineers (SPIE) Conference Series* **9602**, p. 960209, Sept. 2015.
 3. J. Dalcanton, S. Seager, S. Aigrain, S. Battel, N. Brandt, C. Conroy, L. Feinberg, S. Gezari, O. Guyon, W. Harris, C. Hirata, J. Mather, M. Postman, D. Redding, D. Schiminovich, H. P. Stahl, and J. Tumlinson, "From Cosmic Birth to Living Earths: The Future of UVOIR Space Astronomy," *ArXiv e-prints*, July 2015.
 4. L. Pueyo and C. Norman, "High-contrast Imaging with an Arbitrary Aperture: Active Compensation of Aperture Discontinuities," *ApJ* **769**, p. 102, June 2013.
 5. R. Soummer, A. Sivaramakrishnan, L. Pueyo, B. Macintosh, and B. R. Oppenheimer, "Apodized Pupil Lyot Coronagraphs for Arbitrary Apertures. III. Quasi-achromatic Solutions," *ApJ* **729**, p. 144, Mar. 2011.
 6. O. Guyon, P. M. Hinz, E. Cady, R. Belikov, and F. Martinache, "High Performance Lyot and PIAA Coronagraphy for Arbitrarily Shaped Telescope Apertures," *ApJ* **780**, p. 171, Jan. 2014.
 7. A. Sivaramakrishnan, C. D. Koresko, R. B. Makidon, T. Berkefeld, and M. J. Kuchner, "Ground-based Coronagraphy with High-order Adaptive Optics," *ApJ* **552**, pp. 397–408, May 2001.
 8. M. J. Kuchner and W. A. Traub, "A Coronagraph with a Band-limited Mask for Finding Terrestrial Planets," *ApJ* **570**, pp. 900–908, May 2002.
 9. O. Guyon, "Phase-induced amplitude apodization of telescope pupils for extrasolar terrestrial planet imaging," *A&A* **404**, pp. 379–387, June 2003.
 10. W. A. Traub and R. J. Vanderbei, "Two-Mirror Apodization for High-Contrast Imaging," *ApJ* **599**, pp. 695–701, Dec. 2003.
 11. O. Guyon, E. A. Pluzhnik, R. Galicher, F. Martinache, S. T. Ridgway, and R. A. Woodruff, "Exoplanet Imaging with a Phase-induced Amplitude Apodization Coronagraph. I. Principle," *ApJ* **622**, pp. 744–758, Mar. 2005.
 12. A. Sivaramakrishnan and N. Yaitskova, "Lyot Coronagraphy on Giant Segmented-Mirror Telescopes," *ApJL* **626**, pp. L65–L68, June 2005.
 13. R. Soummer, "Apodized Pupil Lyot Coronagraphs for Arbitrary Telescope Apertures," *ApJL* **618**, pp. L161–L164, Jan. 2005.
 14. D. C. Moody, B. L. Gordon, and J. T. Trauger, "Design and demonstration of hybrid Lyot coronagraph masks for improved spectral bandwidth and throughput," in *Space Telescopes and Instrumentation 2008: Optical, Infrared, and Millimeter, Society of Photo-Optical Instrumentation Engineers (SPIE) Conference Series* **7010**, p. 70103P, July 2008.
 15. E. Cady, "Design of Mirrors and Apodization Functions in Phase-induced Amplitude Apodization Systems," *ApJs* **201**, p. 25, Aug. 2012.
 16. J. Trauger, D. Moody, B. Gordon, J. Krist, and D. Mawet, "Complex apodization Lyot coronagraphy for the direct imaging of exoplanet systems: design, fabrication, and laboratory demonstration," in *Space Telescopes and Instrumentation 2012: Optical, Infrared, and Millimeter Wave, Society of Photo-Optical Instrumentation Engineers (SPIE) Conference Series* **8442**, p. 84424Q, Sept. 2012.
 17. M. N'Diaye, L. Pueyo, and R. Soummer, "Apodized Pupil Lyot Coronagraphs for Arbitrary Apertures. IV. Reduced Inner Working Angle and Increased Robustness to Low-order Aberrations," *ApJ* **799**, p. 225, Feb. 2015.
 18. K. Fogarty, L. Pueyo, J. Mazoyer, and M. N'Diaye, "Polynomial Apodizers for Centrally Obscured Vortex Coronagraphs," *ArXiv e-prints*, Mar. 2017.

19. D. Mawet, E. Serabyn, J. K. Wallace, and L. Pueyo, "Improved high-contrast imaging with on-axis telescopes using a multistage vortex coronagraph," *Optics Letters* **36**, p. 1506, Apr. 2011.
20. D. Mawet, P. Riaud, O. Absil, and J. Surdej, "Annular Groove Phase Mask Coronagraph," *ApJ* **633**, pp. 1191–1200, Nov. 2005.
21. D. Mawet, P. Riaud, C. Hanot, D. Vandormael, J. Loicq, J. Baudrand, J. Surdej, and S. Habraken, "The annular groove phase mask coronagraph: an achromatic optical vortex," in *Society of Photo-Optical Instrumentation Engineers (SPIE) Conference Series, Society of Photo-Optical Instrumentation Engineers (SPIE) Conference Series* **6693**, Sept. 2007.
22. D. Mawet, J. T. Trauger, E. Serabyn, D. C. Moody, Jr., K. M. Liewer, J. E. Krist, D. M. Shemo, and N. A. O'Brien, "Vector vortex coronagraph: first results in the visible," in *Society of Photo-Optical Instrumentation Engineers (SPIE) Conference Series, Society of Photo-Optical Instrumentation Engineers (SPIE) Conference Series* **7440**, Aug. 2009.
23. D. Mawet, E. Serabyn, D. Moody, B. Kern, A. Niessner, A. Kuhnert, D. Shemo, R. Chipman, S. McClain, and J. Trauger, "Recent results of the second generation of vector vortex coronagraphs on the high-contrast imaging testbed at JPL," in *Society of Photo-Optical Instrumentation Engineers (SPIE) Conference Series, Society of Photo-Optical Instrumentation Engineers (SPIE) Conference Series* **8151**, Sept. 2011.
24. J. Mazoyer, L. Pueyo, M. N'Diaye, D. Mawet, R. Soummer, and C. Norman, "Correcting for the effects of pupil discontinuities with the ACAD method," in *Society of Photo-Optical Instrumentation Engineers (SPIE) Conference Series, Society of Photo-Optical Instrumentation Engineers (SPIE) Conference Series* **9904**, p. 99044T, July 2016.
25. G. Ruane, J. Jewell, D. Mawet, L. Pueyo, and S. Shaklan, "Apodized vortex coronagraph designs for segmented aperture telescopes," *ArXiv e-prints*, July 2016.
26. G. Ruane, D. Mawet, J. Jewell, and S. Shaklan, "Performance and sensitivity of vortex coronagraphs on segmented space telescopes," *ArXiv e-prints*, Aug. 2017.
27. J. Mazoyer in prep.
28. D. Mawet, L. Pueyo, D. Moody, J. Krist, and E. Serabyn, "The Vector Vortex Coronagraph: sensitivity to central obscuration, low-order aberrations, chromaticism, and polarization," in *Society of Photo-Optical Instrumentation Engineers (SPIE) Conference Series, Society of Photo-Optical Instrumentation Engineers (SPIE) Conference Series* **7739**, July 2010.
29. C. Jenkins, "Optical vortex coronagraphs on ground-based telescopes," *MNRAS* **384**, pp. 515–524, Feb. 2008.
30. D. Mawet, P. Riaud, O. Absil, and J. Surdej, "Annular Groove Phase Mask Coronagraph," *ApJ* **633**, pp. 1191–1200, Nov. 2005.
31. D. Mawet, L. Pueyo, A. Carlotti, B. Mennesson, E. Serabyn, and J. K. Wallace, "Ring-apodized Vortex Coronagraphs for Obscured Telescopes. I. Transmissive Ring Apodizers," *ApJS* **209**, p. 7, Nov. 2013.
32. K. Fogarty, L. Pueyo, and D. Mawet, "Optimal apodizations for on-axis vector vortex coronagraphs," in *Space Telescopes and Instrumentation 2014: Optical, Infrared, and Millimeter Wave, Society of Photo-Optical Instrumentation Engineers (SPIE) Conference Series* **9143**, p. 914326, Aug. 2014.
33. J. Mazoyer, L. Pueyo, C. Norman, M. N'Diaye, D. Mawet, R. Soummer, M. Perrin, É. Choquet, and A. Carlotti, "Active correction of aperture discontinuities (ACAD) for space telescope pupils: a parametric analysis," in *Techniques and Instrumentation for Detection of Exoplanets VII, Society of Photo-Optical Instrumentation Engineers (SPIE) Conference Series* **9605**, p. 96050M, Sept. 2015.